Inorganic Chemistry

Article

pubs.acs.org/IC

Effect of Pillar Modules and Their Stoichiometry in 3D Porous Frameworks of Zn(II) with $[Fe(CN)_6]^{3-}$: High CO_2/N_2 and CO_2/CH_4 Selectivity

Arpan Hazra, Satyanarayana Bonakala, Sandeep K. Reddy, Sundaram Balasubramanian,* and Tapas Kumar Maji*

Chemistry and Physics of Materials Unit, Jawaharlal Nehru Centre for Advanced Scientific Research, Jakkur, Bangalore, 560 064, India

Supporting Information

ABSTRACT: We report the synthesis, single-crystal structural characterization, and selective gas adsorption properties of three new 3D metal−organic frameworks of Zn(II), $\{[Zn_3(bipy)_3(H_2O)_2][Fe(CN)_6]_2\cdot 2(bipy)\cdot 3H_2O\}_n$ (**1**), $\{[Zn_3(bipy)][Fe(CN)_6]_2\cdot(C_2H_5OH)\cdot H_2O\}_n$ (**2**), and $\{[Zn_3(azpy)_2(H_2O)_2][Fe(CN)_6]_2\cdot 4H_2O\}_n$ (**3**) (bipy = 4,4′-bipyridyl and azpy = 4,4′-azobipyridyl), bridged by $[Fe(CN)_6]^{3-}$ and exobidentate pyridyl-based linkers. Compounds **1**−**3** have been successfully isolated by varying the organic linkers (bipy and azpy) and their ratios during the synthesis at RT. Frameworks **1** and **3** feature a biporous-type network. At 195 K, compounds **1**−**3** selectively adsorb CO_2 and completely exclude other small molecules, such as N_2, Ar, O_2, and CH_4. Additionally, we have also tested the CO_2 uptake capacity of **1** and **3** at ambient temperatures. By using the isotherms measured at 273 and 293 K, we have calculated the isosteric heat of CO_2 adsorption, which turned out to be 35.84 and 35.53 kJ mol^{-1} for **1** and **3**, respectively. Furthermore, a reasonably high heat of H_2 adsorption (7.97 kJ mol^{-1} for **1** and 7.73 kJ mol^{-1} for **3**) at low temperatures suggests strong interaction of H_2 molecules with the unsaturated Zn(II) metal sites and as well as with the pore surface. Frameworks **1** and **3** show high selectivity to CO_2 over N_2 and CH_4 at 273 K, as calculated based on the IAST model. The high values of ΔH_{CO_2} and ΔH_{H_2} stem from the preferential electrostatic interaction of CO_2 with the unsaturated metal sites, pendent nitrogen atoms of $[Fe(CN)_6]^{3-}$, and π-electron cloud of bipyridine aromatic rings as understood from first-principles density functional theory based calculations.

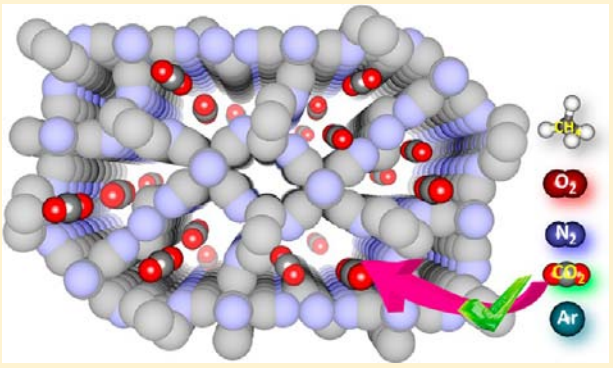

INTRODUCTION

Metal−organic frameworks (MOFs) or porous coordination polymers (PCPs)[1] are a class of crystalline porous materials and have several advantages, such as tunable surface area, feasibility of modifiable pore size, and modular nature of pore environment compared to traditional zeolites and carbon-based materials.[2] All of these characteristics along with the flexible organic/inorganic linkers and variable geometry of metal ions with moderate coordination bond energy place the framework materials in the cutting edge for clean energy research, such as storage and separation of hydrogen (H_2)[3] and carbon dioxide (CO_2),[4] and other advanced applications, such as drug delivery, sensing, and catalysis.[5] Among the alternative energy sources, H_2 stands at the forefront due to its clean combustion and high gravimetric energy density,[6] but its application is restricted due to the lack of efficient storage materials. Therefore, the target is to synthesize lightweight and cost-effective materials that can reversibly store H_2 at near ambient temperature.[7] Theoretical calculations have predicted the ideal binding energy to be around 20−25 kJ/mol[8] for room-temperature storage in a solid adsorbent under a working pressure of 30 bar. To increase the storage capacity and binding energy (ΔH_{H_2}) in MOFs, several approaches have been documented, such as immobilization of alkali metal cations,[9] exposure of unsaturated metal sites (UMSs)[10] and highly electronegative heteroatoms embedded linkers on the pore surface,[11] reduction of pore size via interpenetration and molecular spill over.[3d,11,12] We envisage a further increase of the ΔH_{H_2} value through interaction sites, such as UMSs along with functional polar groups or heteroatoms decorated on the pore surface. However, the increase of density of such interaction sites in a framework material is a highly demanding and challenging task. On the other hand, selective capture and storage of greenhouse gas CO_2 from precombustion natural gas or postcombustion flue gas are of paramount importance for energy and the environment.[13] As CO_2 is often found as a major impurity in natural gas and its presence can reduce the efficiency, therefore, a material for selective capture with high efficiency of CO_2 from methane (CH_4) is highly sought-after.[14] Furthermore, developments of viable carbon capture and

Received: June 28, 2013
Published: September 13, 2013

   dx.doi.org/10.1021/ic401657d | *Inorg. Chem.* 2013, 52, 11385−11397

Scheme 1. Effect of Pillar Modules and Their Stoichiometry Toward the Formation of Three 3D Porous Frameworks of Zn(II) with $[Fe(CN)_6]^{3-}$

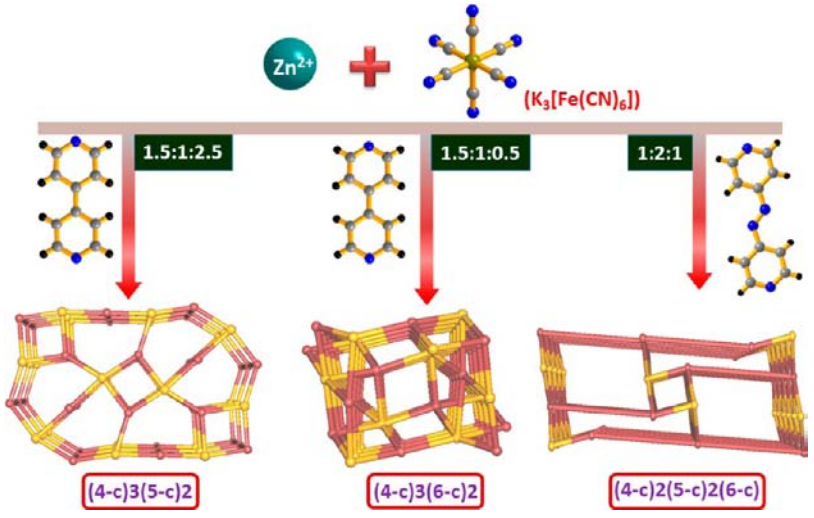

sequestration technologies (CCSTs) pose a significant challenge in the current environmental context. The percentage of N_2 in flue gas is more than 70%. Therefore, synthesis of CO_2 selective materials over N_2 is of prime importance. CO_2 is a polar molecule with a large quadruple moment; therefore, a tunable pore surface with high electronegative atoms or UMSs would be one of the key approaches for this purpose.

Our group has been extensively working on the design and synthesis of MOF-based materials for H_2 storage with a high heat of adsorption and selective capture and storage of CO_2.[1S] Recently, we have adopted a strategy to build multifunctional MOFs using hexacyanometallate $[M(CN)_6]^{3-}$ as a metallo-ligand that has been extensively investigated for the fabrication of molecule-based magnetic material.[1Sh,i] In our strategy, four equatorial CN^- groups of $[M(CN)_6]^{3-}$ could connect with metal ions to build a 2D network, which can be further pillared by rigid organic exobidentate linkers to attain a 3D pillared-layer framework. We envisioned that this approach would provide a framework with UMSs and free uncoordinated axial −CN groups in the pore surface that effectively increase the density of adsorption sites on the pore surface. Recently, we have achieved a high heat of H_2 adsorption in such a bifunctional pillar layered framework of Mn(II) with $[Cr(CN)_6]^{3-}$ and bipy.[1Sh]

In the present work, we have chosen $[Fe(CN)_6]^{3-}$ as a metallo-ligand to connect with Zn(II) to build a 2D network, which has been extended to 3D by selecting suitable pillars. The capability of Zn(II) to adopt a versatile geometry makes it a widely adorable metal for the construction of porous frameworks (Scheme 1). We have also carefully tuned the concentration of linker bipy to investigate the change in structural topology as well as the overall porosity in the framework. To invoke greater porosity with enhanced polarity in the framework, we have changed bipy to the longer azpy with an azo (−N═N−) functional group in the backbone, and such a linker would generate a nitrogen phobic pore surface with improved CO_2 uptake properties. In this Article, we report the synthesis, structural versatility, and gas storage properties of three different MOFs, $\{[Zn_3(bipy)_3(H_2O)_2][Fe(CN)_6]_2\cdot 2(bipy)\cdot 3H_2O\}_n$ (**1**), $\{[Zn_3(bipy)][Fe(CN)_6]_2\cdot(C_2H_5OH)\cdot H_2O\}_n$ (**2**), and $\{[Zn_3(azpy)_2(H_2O)_2][Fe(CN)_6]_2\cdot 4H_2O\}_n$ (**3**) (bipy = 4,4′-bipyridyl and azpy = 4,4′-azobipyridyl), obtained at RT. The microscopic nature of interactions between the gas molecules and the frameworks has been elucidated using dispersion-corrected density functional theory calculations.

EXPERIMENTAL SECTION

Materials. All the reagents and solvents employed were commercially available and used as supplied without further purification. $K_3[Fe(CN)_6]$, 4,4′-bipyridine (bipy), and $Zn(NO_3)_2\cdot 6H_2O$ were obtained from the Aldrich Chemical Co. 4,4′-Azobipyridine (azpy) had been synthesized according to the literature procedure.[16] ***Caution!*** *Cyanide-containing compounds are potentially toxic and should be handled very carefully.*

Synthetic Procedure. *Synthesis of* $\{[Zn_3(bipy)_3(H_2O)_2][Fe(CN)_6]_2\cdot(bipy)\cdot 3H_2O\}_n$ ***(1).*** An aqueous solution (12.5 mL) of $K_3[Fe(CN)_6]$ (0.25 mmol) was added to an ethanolic solution (12.5 mL) of bipy (0.5 mmol), and the mixture was stirred for 30 min. $ZnCl_2$ (0.25 mmol) was dissolved in 12.5 mL of distilled water, and 2.5 mL of this metal solution was carefully layered with the 2.5 mL of mixed bipy and $K_3[Fe(CN)_6]$ solution using an ethanol/water buffer solution (1 mL, 1:1) in a test tube. After 15 days, yellow colored block-shaped crystals appeared in the middle of the tube and were separated and washed with ethanol. The bulk amount of the sample was prepared by the direct mixing of the respective reagents in ethanol−water solution under stirring for 24 h, and the phase purity was checked with the PXRD and elemental analysis. Yield: 77%, relative to Fe. Anal. Calcd for $C_{62}H_{50}Fe_2Zn_3N_{22}O_5$: C, 49.94; H, 3.38; N, 20.66. Found: C, 49.84; H, 3.48; N, 20.48. IR (KBr, cm^{-1}): $\nu(H_2O)$ 3490, 3426; ν(ArC-H) 3064, 3054; $\nu(C\equiv N)$ 2162, 2098; ν(ArC═C) 1609, 1537. The IR spectrum of **1** (Figure S2, Supporting Information) shows strong and broad bands around 3490 cm^{-1}, suggesting the presence of water molecules. A strong band around 2162 cm^{-1} corroborates the $\nu(C\equiv N)$ stretching frequency, and a band around 1609 cm^{-1} indicates the presence of bipy molecule.

Preparation of $\{[Zn_3(bipy)_3][Fe(CN)_6]_2\}_n$ ***(1′).*** Compound **1′** was prepared by heating compound **1** at 175 °C under vacuum ($<10^{-1}$ Pa) for 72 h. The removal of the guest bipy and water molecules (coordinated and guest) was confirmed by elemental analysis, TGA, and IR spectroscopy. This powdered sample was used for different characterizations. Anal. Calcd for $C_{42}H_{24}Fe_2Zn_3N_{18}$: C, 46.34; H, 2.22; N, 23.16. Found: C, 45.80; H, 2.53; N, 22.86.

Synthesis of $\{[Zn_3(bipy)][Fe(CN)_6]_2\cdot(C_2H_5OH)\cdot H_2O\}_n$ ***(2).*** An aqueous solution (12.5 mL) of $K_3[Fe(CN)_6]$ (0.25 mmol) was added to an ethanolic solution (12.5 mL) of bipy (0.25 mmol), and the mixture was stirred for 30 min. $ZnCl_2$ (0.25 mmol) was dissolved in 12.5 mL of distilled water, and 2.5 mL of this metal solution was

dx.doi.org/10.1021/ic401657d | Inorg. Chem. 2013, 52, 11385−11397

Table 1. Crystallographic Data and Structure Refinement Parameters for Compounds 1−3

	1	2	3
empirical formula	$C_{62}H_{50}Fe_2Zn_3N_{22}O_5$	$C_{24}H_{16}Fe_2Zn_3N_{14}O_2$	$C_{32}H_{28}Fe_2Zn_3N_{20}O_6$
M	1491.07	840.38	1096.58
crystal system	orthorhombic	monoclinic	monoclinic
space group	*Pbam* (No. 55)	*C*2/*c* (No. 15)	*C*2/*m* (No. 12)
a (Å)	15.8354(5)	13.4237(18)	23.1680(17)
b (Å)	17.5204(6)	20.496(2)	7.5344(5)
c (Å)	11.4998(3)	23.570(4)	13.4973(9)
α (deg)	90	90	90
β (deg)	90	98.472(7)	99.799(5)
γ (deg)	90	90	90
V (Å^3)	3190.53(17)	6414.1(15)	2321.7(3)
Z	2	8	2
T (K)	290	290	290
λ (Mo Kα)	0.71073	0.71073	0.71073
D_c (g cm^{-3})	1.552	1.740	1.563
μ (mm^{-1})	1.623	3.141	2.199
$\theta_{max}/\theta_{min}$ (deg)	26.0/1.7	22.5/1.8	25.0/2.8
total data	34 783	25 070	10 514
unique reflection	3303	4196	2203
R_{int}	0.139	0.247	0.142
data [$I > 2\sigma(I)$]	2313	1927	1166
R^a	0.0415	0.0742	0.0640
$R_w{}^b$	0.0967	0.2108	0.1760
GOF	1.03	0.99	1.02
$\Delta\rho$ min/max [e Å^{-3}]	−0.64, 0.58	−0.82, 0.91	−0.99, 0.93

$^a R = \sum||F_o| - |F_c||/\sum|F_o|$. $^b R_w = [\sum\{w(F_o^2 - F_c^2)^2\}/\sum\{w(F_o^2)^2\}]^{1/2}$.

carefully layered with the 2.5 mL of mixed bipy and $K_3[Fe(CN)_6]$ solution using an ethanol/water buffer solution (1 mL, 1:1) in a crystal tube. After 30 days, light yellow colored block-shaped crystals appeared in the middle of the tube and were separated and washed with ethanol (Yield: ∼60%). A different procedure was employed for the preparation of the sample in bulk amount. An aqueous solution (12.5 mL) of $K_3[Fe(CN)_6]$ (0.16 mmol) was added to an ethanolic solution (12.5 mL) of bipy (0.08 mmol), and the mixture was stirred for 30 min. This resulting solution was added dropwise to a solution of $ZnCl_2$ (0.25 mmol), and the mixture was stirred for 36 h. The phase purity was checked with the PXRD and elemental analysis. Yield: 57%, relative to Fe. Anal. Calcd for $C_{24}H_{16}Fe_2Zn_3N_{14}O_2$: C, 34.31; H, 1.92; N, 23.34. Found: C, 34.10; H, 1.79; N, 23.27. IR (KBr, cm^{-1}): ν(H_2O) 3653, 3572; ν(ArC-H) 3107, 2982; ν(C≡N) 2197, 2157, 2090; ν(ArC=C) 1618, 1563. The IR spectrum of **2** (Figure S3, Supporting Information) shows strong and sharp bands around 3653 cm^{-1}, suggesting the presence of water molecules. A strong band around 2090 cm^{-1} corroborates the ν(C≡N) stretching frequency, and a band around 1618 cm^{-1} indicates the presence of bipy molecule.

Preparation of $\{[Zn_3(bipy)][Fe(CN)_6]_2\}_n$ ***(2′)***. Compound **2′** was prepared by heating compound **2** at 130 °C under vacuum (<10^{-1} Pa) for 72 h. The removal of the guest ethanol and water molecules was confirmed by elemental analysis, TGA, and IR spectroscopy. This powdered sample was used for characterization of different physical properties. Anal. Calcd for $C_{22}H_8Fe_2Zn_3N_{14}$: C, 34.21; H, 1.04; N, 25.40. Found: C, 34.82; H, 1.15; N, 24.86.

Synthesis of $\{[Zn_3(azpy)_2(H_2O)_2][Fe(CN)_6]_2{\cdot}4H_2O\}_n$ ***(3)***. Compound **3** was synthesized adopting a similar procedure as that of **1**, where we have used azpy instead of bipy. The different stoichiometry was employed where $K_3[Fe(CN)_6]$ and azpy were taken as 0.5 and 0.25 mmol, respectively. After 15 days, orange-yellow colored block crystals appeared in the middle of the tube and were separated and washed with ethanol (Yield: ∼60%). The bulk amount of the sample was prepared by the direct mixing of the reagents in ethanol/water mixed solution with stirring for 24 h, and the phase purity was checked with the PXRD and elemental analysis. Yield: 80%, relative to Fe. Anal. Calcd for $C_{32}H_{28}Fe_2Zn_3N_{20}O_6$: C, 35.05; H, 2.57; N, 25.54. Found: C, 35.87; H, 2.55; N, 25.37. IR (KBr, cm^{-1}): ν(H_2O) 3662, 3576, 3427 (broad); ν(ArC-H) 3091; ν(C≡N) 2168, 2098; ν(ArC=C) 1607, 1571. The IR spectrum of **3** (Figure S4, Supporting Information) shows strong and sharp peaks around 3662 and 3576 cm^{-1}, suggesting the presence of water molecules. A strong band around 2168 cm^{-1} corroborates the ν(C≡N) stretching frequency, and a band around 1607 cm^{-1} indicates the presence of azpy molecule.

Preparation of $\{[Zn_3(azpy)_2][Fe(CN)_6]_2\}_n$ ***(3′)***. Compound **3′** was prepared by heating compound **3** at 160 °C under vacuum (<10^{-1} Pa) for 72 h. The removal of the water molecules (coordinated and guest) was confirmed by elemental analysis, TGA, and IR spectroscopy. This powdered sample was used for characterization of different physical properties. Anal. Calcd for $C_{32}H_{14}Fe_2Zn_3N_{20}$: C, 39.11; H, 1.43; N, 28.52. Found: C, 38.91; H, 1.53; N, 28.37.

Physical Measurements. The elemental analyses of each compound and their corresponding dehydrated phases were carried out on a Thermo Fisher Flash 2000 Elemental Analyzer. Fourier transformed IR spectroscopic studies were carried out using a KBr pellet (Bruker IFS-66v). Thermogravimetric analysis (TGA) was carried out (Metler Toledo) in a nitrogen atmosphere (flow rate = 50 mL min^{-1}) in the temperature range of 30−650 °C (heating rate = 2 °C min^{-1}). Powder XRD patterns of the products were recorded by using Cu-Kα radiation (Bruker D8 Discover; 40 kV, 30 mA).

Single-Crystal X-ray Diffraction. Suitable single crystals of compounds **1**−**3** were mounted on a thin glass fiber with commercially available super glue. X-ray single-crystal structural data were collected on a Bruker Smart-CCD diffractometer equipped with a normal focus and a 2.4 kW sealed tube X-ray source with graphite monochromated Mo-Kα radiation (λ = 0.71073 Å) operating at 50 kV and 30 mA. The program SAINT[17] was used for the integration of diffraction profiles, and absorption correction was made with the SADABS[18] program. All the structures were solved by SIR 92[19] and refined by the full-matrix least-squares method using SHELXL.[20] All the hydrogen atoms were fixed by HFIX and placed in ideal positions. The potential solvent accessible area or void space was calculated using the PLATON[21] multipurpose crystallographic software. All crystallographic and structure refinement data of **1**−**3** are summarized in Table 1. Selected

dx.doi.org/10.1021/ic401657d | *Inorg. Chem.* 2013, 52, 11385−11397

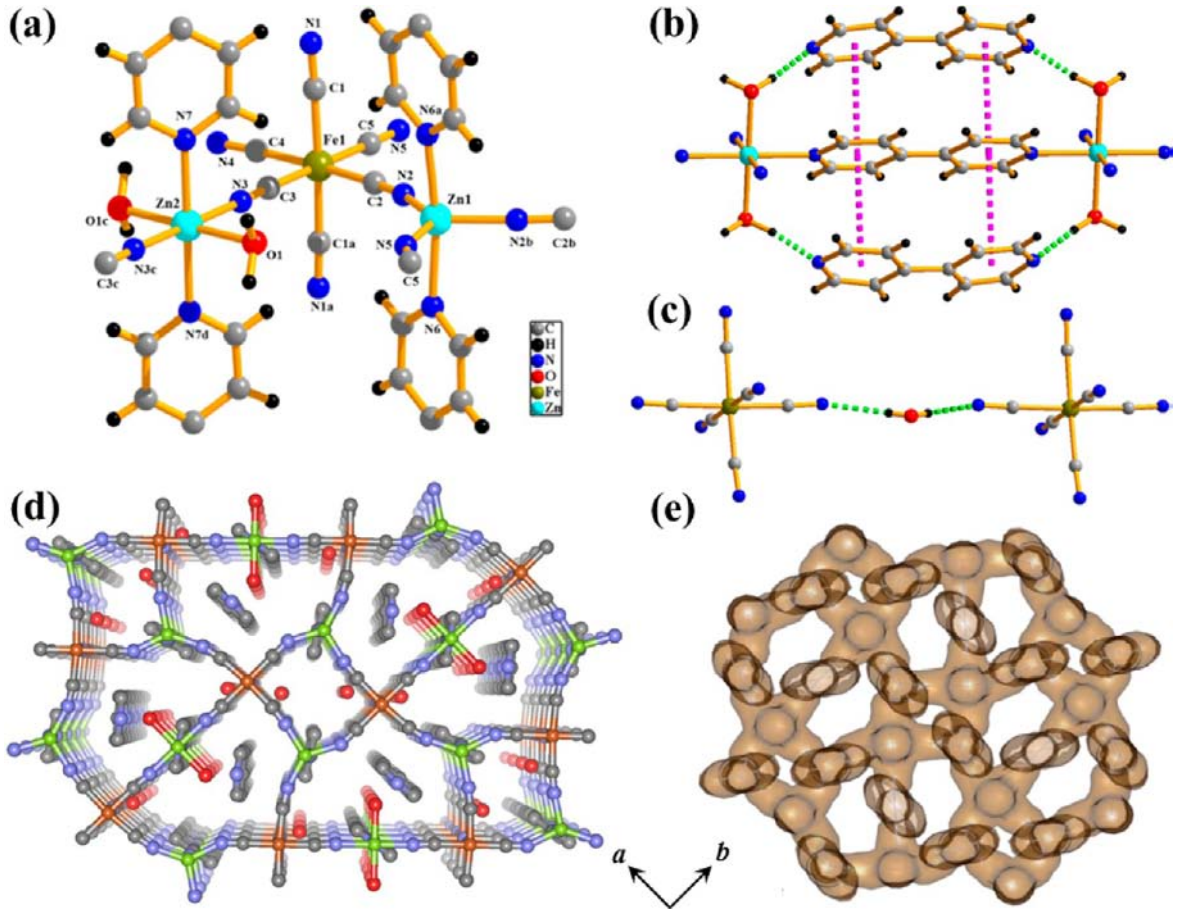

Figure 1. (a) View of the coordination environment of Zn(II) (Zn1 and Zn2 atoms) in **1**. (Symmetry codes: $a = x, y, -z$; $b = 0.5 - x, 0.5 + y, -z$; $c = -x, -y, z$; and $d = -x, -y, -z$). (b) H-bonding interaction between coordinated water and guest bipy molecules. Guest and coordinated bipy molecules are also involved in $\pi\cdots\pi$ interactions. (c) One guest water molecule in the pore interacts with pendent CN groups from two layers via N$\cdots$H−O hydrogen-bonding interactions. (d) 3D pillared layer framework of **1** viewed along the *c* direction showing two different types of channels occupied guest water and bipy molecules. (e) View of the biporous structure after removing the guest and coordinated water molecules.

bond lengths and angles for compounds **1**−**3** are given in Tables S3−S8 (Supporting Information). All calculations were carried out using SHELXL 97,[20] PLATON,[21] SHELXS 97,[20] and WinGX system, Ver 1.80.05.[22] The guest water molecules of compound **3** were found to be disordered and were solved by changing the occupancy.

Adsorption Study. N_2 (77 K, 195 and 273 K), H_2 (77 and 87 K), CO_2 (195 K, 273 and 293 K), Ar (195 K), CH_4 (273 K), and O_2 (195 K) adsorption studies were carried out with the desolvated samples, that is, **1′**−**3′** by using a QUANTACHROME QUADRASORB SI analyzer and an AUTOSORB IQ2 instrument. High-pressure hydrogen adsorption isotherm measurements at 77 K were carried out on a fully computer-controlled volumetric BELSORP-HP, BEL JAPAN high-pressure instrument. All the gases used for adsorption measurement are of scientific/research grade with 99.999% purity. The water adsorption at 298 K was measured for all the compounds in the vapor state by using a BELSORP-aqua-3 analyzer. Water molecules used to generate the vapor were degassed fully by repeated evacuation. Dead volume was measured with helium gas. Adsorbent samples weighing around 100−150 mg were placed in the sample tube. All operations were computer-controlled and automatic. Prior to the measurement of the isotherms, the samples were desolvated for about 72 h under high-vacuum conditions (<0.1 Pa) at different temperatures: 175 °C to obtain **1′**, 130 °C for **2′**, and 160 °C to obtain **3′**.

Computational Details. To find the position of a gas molecule inside the MOF, density functional theory calculations were carried out using the QUICKSTEP module in CP2K software.[23] All valence electrons were treated in a mixed basis set with an energy cutoff of 280 Ry. The short-range version of the double-ζ single polarization basis set was used. The effect of core electrons and nuclei was considered by using pseudopotentials of Goedecker−Teter−Hutter (GTH).[24] The exchange and correlation interaction between electrons was treated with the Perdew−Burke−Ernzerhof (PBE)[25] functional. Because van der Waals interactions between the gas and the framework are very important, their effects were accounted for by employing empirical corrections developed by Grimme. Two schemes, DFT-D2[26] and DFT-D3,[27] were used to calculate the cell volume and binding energy. The effect of the exchange-correlation functional was also examined by replacing the PBE functional with those of Becke−Lee−Yang−Parr (BLYP).[28] The simulation cell consisted of $1 \times 1 \times 1$ unit cell for **1′** and $1 \times 2 \times 1$ unit cells for **3′**. As discussed before, both compounds contain coordinatively unsaturated Zn atom sites in the framework. Compound **1′** contains two open metal sites, whereas compound **3′** contains one open metal site.

Calculations using the PBE functional best reproduced the experimental cell parameters. van der Waals corrections (both D2 and D3 types) overestimated the sample density systematically,[29] with D3 performing relatively better than D2. The cell parameters calculated via all of these methods are summarized in Tables S1 and S2 in the Supporting Information. However, for calculating the binding energy between the gas molecule and organic linkers of the MOF, vdW corrections were found to be essential. In this regard, the D3 set performs the best for a comparison to experimentally determined enthalpies of adsorption.

The binding energy of gas was calculated as

$$\Delta E = E_{(\mathrm{MOF+gas})} - E_{(\mathrm{MOF})} - E_{(\mathrm{gas})}$$

dx.doi.org/10.1021/ic401657d | *Inorg. Chem.* 2013, 52, 11385−11397

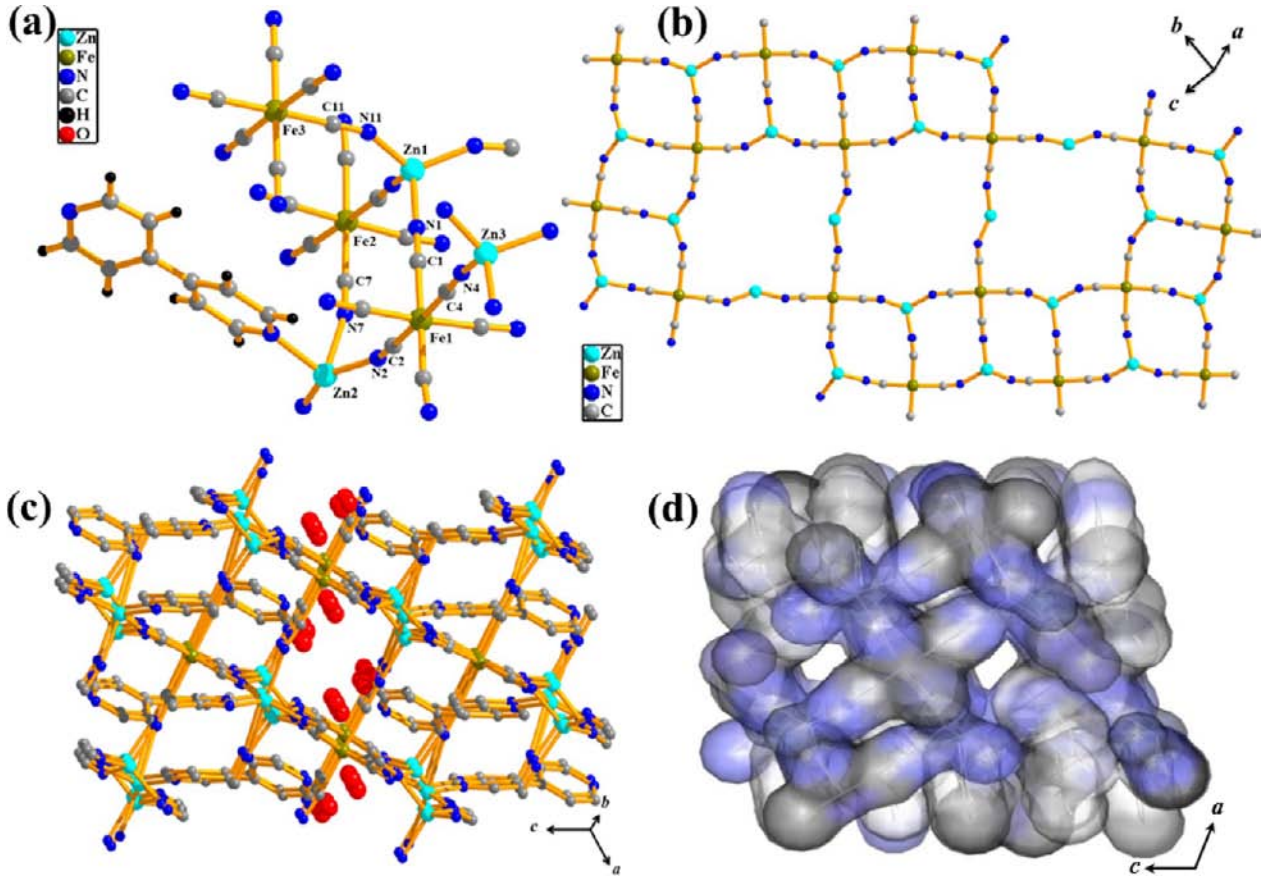

Figure 2. (a) View of the coordination environment of three Zn atoms present in the asymmetric unit in **2**. (b) View of the 2D sheet along the (101) plane, which is constructed by metal and cyanide bridging. (c) View of 3D architecture of compound **2** along the *b* direction showing pendent bipy molecules. Water molecules (red colored balls) are occupying in the 1D channel. (d) View of the pores in **2** along the *b* direction.

Here, $E_{(MOF+gas)}$ is the energy of the MOF with H_2 or CO_2, $E_{(MOF)}$ is the energy of the MOF, and $E_{(gas)}$ is the energy of the isolated gas molecule. The energy of an isolated gas molecule was calculated in the same simulation box size as that of the MOF. The energies were corrected for the basis set superposition error (BSSE) using the counterpoise method. All structures were visualized using VMD,[30] Mercury,[31] and GaussView.[32]

RESULTS AND DISCUSSION

Structural Description of $\{[Zn_3(bipy)_3(H_2O)_2][Fe(CN)_6]_2\cdot 2(bipy)\cdot 3H_2O\}_n$ (1). Single-crystal X-ray crystallographic structure determination reveals that **1** is a neutral 3D coordination architecture of Zn(II) built of $[Fe(CN)_6]^{3-}$ and bipy with the formula of $\{[Zn_3(bipy)_3(H_2O)_2][Fe(CN)_6]_2\cdot 2(bipy)\cdot 3H_2O\}_n$. Compound **1** crystallizes in the orthorhombic system in the *Pbam* space group. There are two crystallographically independent Zn (Zn1 and Zn2) atoms in the asymmetric unit where each octahedral Zn2 is coordinated to two CN groups from two $[Fe(CN)_6]^{3-}$, two bipy, and two water molecules (O1, O1c), whereas each trigonal-bipyramidal Zn1 is coordinated to three CN groups from three different $[Fe(CN)_6]^{3-}$ and two bipy molecules (Figure 1a). The Zn−N and Zn−O bond distances are in the ranges of 2.983−2.220 and 2.079−2.186 Å. In the 2D layer, the 12-membered $Zn1_2Fe1_2(CN)_4$ ring is surrounded by six 18-membered $Zn1Zn2_2Fe1_3(CN)_{12}$ rings and each 2D layer is connected by the bipy linker through the Zn(II) centers, forming a 3D pillared-layer framework with two kinds of channels along the *c* axis (Figure 1d). Examination with TOPOS[33] reveals that **1** is a trinodal (4-c)3(5-c)2-periodic 3D net formed by 5-connected (5-c) Zn-nodes, (4-c) Fe-nodes. In a layer, the vertex symbol for Zn1, Zn2, and Fe1 points are represented by Schläfli symbols, $\{4.6^8.8\}$, $\{6^5.8\}$, and $\{4.6^5\}$, respectively. Further examination shows that **1** adopts a topology with the Schläfli symbol $\{4.6^5\}_2\{4.6^8.8\}_2\{6^5.8\}$. After removing the coordinated and guest molecules (H_2O and bipy), compound **1** offers a biporous network with open channels along the crystallographic *c* direction (Figure 1e). The rectangular-shaped voids are observed along *c* with the diameter of 5.9 × 4.1 $Å^2$ (Figure 1e). Upon removal of the coordinated water and guest (water, bipy) molecules, the framework shows 37.9% void space to the total volume with coordinatively unsaturated Zn(II) centers on the pore surface (Figure S1, Supporting Information). The guest water molecules O1w and O2w are H-bonded (O1w···O2w, 2.975 Å) to each other, and O1w is also making a bridge between the two layers through N1 of the pendant CN group (N1···O1w, 2.918 Å) (Figure 1c). The guest bipy molecules undergoes strong face-to-face $\pi\cdots\pi$ interactions (Figure 1b) with two different coordinated bipy (cg···cg distances are in the range of 3.631−3.905 Å) linkers connected to two Zn (Zn1 and Zn2) centers. In the 3D network, separation between the layers through Zn(II)−bipy−Zn(II) is 11.628 Å, whereas, in the 2D layer, the Zn1−Fe1 and Zn2−Fe1 distances are 5.044 and 5.143 Å, respectively.

Structural Description of $\{[Zn_3(bipy)][Fe(CN)_6]_2\cdot C_2H_5OH\cdot H_2O\}_n$ (2). X-ray single-crystal structure determination reveals that compound **2** crystallizes in the monoclinic

dx.doi.org/10.1021/ic401657d | *Inorg. Chem.* 2013, 52, 11385−11397

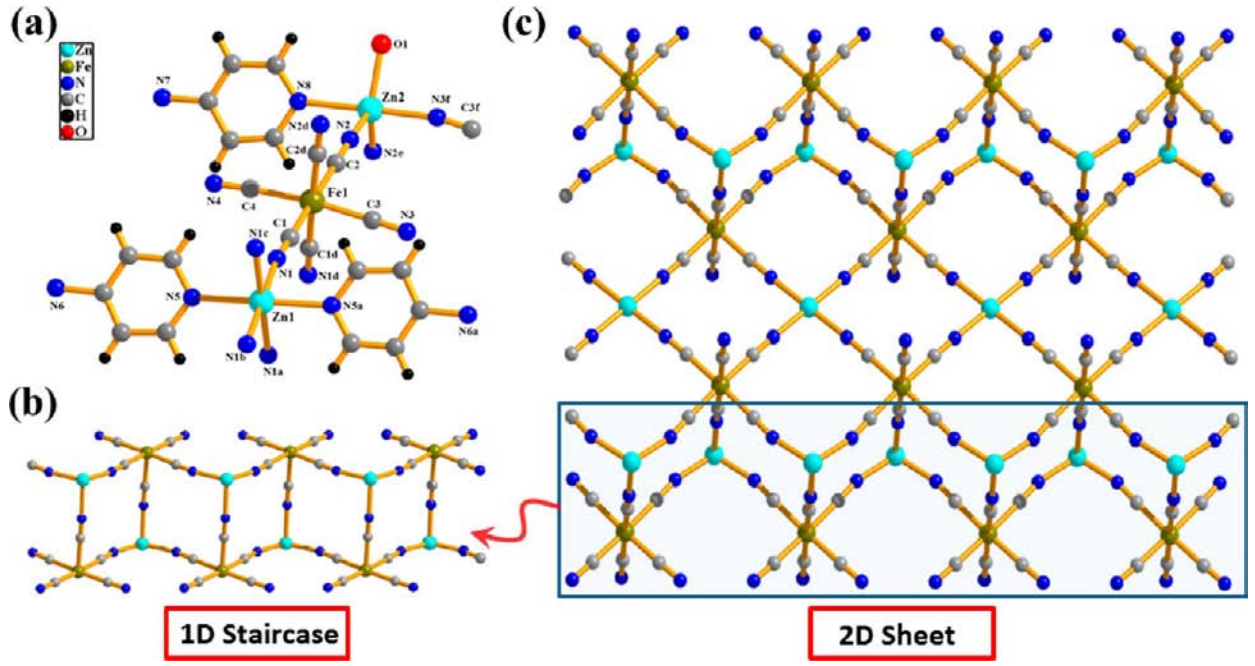

Figure 3. (a) View of the coordination environment of Zn(II) atoms connected by $[Fe(CN)_6]^{3-}$ and azpy in **3**. Symmetry code: $a = 1 - x, y, -z$; $b = 1 - x, 1 - y, -z$; $c = x, 1 - y, z$; $d = x, 2 - y, z$; $e = x, 3 - y, z$; and $f = 1.5 - x, 0.5 + y, -z$. (b) 1D staircase-type chain formed by the Zn(II) and $[Fe(CN)_6]^{3-}$. (c) 1D chains are linked with each other by another Zn(II) center to form a 2D corrugated sheet in the *ab* plane.

system in the *C*2/*c* space group and is a 3D coordination framework built of Zn(II), $[Fe(CN)_6]^{3-}$, and bipy, where the latter acts as a monodentate pendant ligand. There are three types of Zn(II) and three types of Fe(III) centers present in the structure, and they are crystallographically independent (Figure 2a). All Fe(III) centers are distorted from ideal octahedral geometry, which is clearly reflected from Fe−C−Fe *cisoid* angles (87.3(7)−93.3(7)° for Fe1, 86.5(8)−94.2° for Fe2, and 87.4(7)−95.1(7)° for Fe3 centers). Fe−C bond lengths are in the range of 1.880(19)−2.22(2) Å. Zn1 and Zn3 centers have a slightly distorted tetrahedral geometry and are connected with four nitrogen atoms from four different cyanides. The degree of distortion is revealed in N−Zn−N angles (103.3(6)−117.9(6)°). Zn−N (Zn1 and Zn3) bond lengths are in the range of 1.924(14)−1.990(16) Å. The Zn2 center has a distorted trigonal-bipyramidal geometry, and the coordination number is fulfilled by five nitrogen atoms from four different cyanide ligands and one pendent bipy molecule (Figure 2a). The distorted geometry is reflected from *cisoid* (104.7(6)−147.2(6)°) and *transoid* (84.3(6)−100.3(6)°) angles of the Zn2 center. Zn−N bond lengths vary from 1.944(15) to 2.430(17) Å. The bipy molecule is connected with the Zn2 center through the nitrogen atom where the other noncoordinating pyridyl end is interacting with the guest C_2H_5OH molecule through H-bonding. The metal ions are connected by the cyanide ligand and thus form a 2D sheet along the [101] direction (Figure 2b). These 2D sheets are further linked by the cyanide ligand along the perpendicular direction of the (101) plane, which leads to the 3D architecture (Figure 2c). Examination with TOPOS[33] reveals that **2** is a hexa-nodal (4-c)3(6-c)2 3D periodic net formed by 6-connected (6-c) Fe-nodes and 4-connected (4-c) Zn-nodes. Among the six different nodes, the vertex symbols for Fe1, Fe2, Fe3 and Zn1, Zn2, Zn3 are represented by Schläfli symbols, $\{4^7.6^8\}$, $\{4^7.6^6.8^2\}$, $\{4^7.6^8\}$ and $\{4^5.6\}$, $\{4^5.6\}$, $\{4^4.6^2\}$, respectively. Further examination shows that **2** adopts an unprecedented network topology with the Schläfli symbol $\{4^4.6^2\}_2\{4^5.6\}_4\{4^7.6^6.8^2\}\{4^7.6^8\}_3$. The guest solvent molecules (O1w and C_2H_5OH) are linked with each other through H-bonding and placed themselves in a 1D channel along the crystallographic *b* direction (Figure 2c). Upon removal of the guest molecules, the framework shows 18% void space to the total unit cell volume (Figure 2d).

Structural Description of $\{[Zn_3(azpy)_2(H_2O)_2][Fe(CN)_6]_2\cdot 4H_2O\}_n$ (3). Compound **3** crystallizes in the monoclinic *C*2/*m* space group, and single-crystal structure determination reveals a neutral 3D coordination architecture of Zn(II) built of $[Fe(CN)_6]^{3-}$ and azpy with the formulation of $\{[Zn_3(azpy)_2(H_2O)_2][Fe(CN)_6]_2\cdot 4H_2O\}_n$. There are two crystallographically independent Zn(II) atoms (octahedral Zn1 and trigonal-bipyramidal Zn2) in the asymmetric unit, and each octahedral Zn1 is coordinated to four nitrogen atoms from different $[Fe(CN)_6]^{3-}$ and another two nitrogen atoms from two azpy linkers. Each trigonal-bipyramidal Zn2 is coordinated to three nitrogen atoms from three $[Fe(CN)_6]^{3-}$, one azpy (N8), and one water molecule (O1) (Figure 3a). Zn1 is slightly distorted from the perfect octahedron, as reflected in the *cisoid* angles (88.63−91.37)°. The Zn−N bond distances are in the range of 2.127−2.245 Å, and the Zn−O bond distance is 2.037 Å. Fe1 and Zn2 centers are connected by cyanide bridges, forming a 12-membered square-shaped ring that extends along the *b* direction, resulting in a 1D staircase-type structure (Figure 3b). Such 1D staircase chains are connected through cyanide linkers and Zn1 centers, leading to a wavy-like 2D sheet in the crystallographic *ab* plane (Figure 3c). Along the *c* direction, these 2D sheets look like a staircase that is further pillared by azpy linker, leading to a 3D framework with 2D channels occupied by guest water molecules (Figure 4a,b). Examination with TOPOS[33] reveals that **3** is a trinodal (4-c)2(5-c)2(6-c)-periodic 3D net formed by 4-connected (4-c), 6-connected (6-c) Zn-nodes and 5-connected (5-c) Fe-nodes. In a 1D chain, the vertex symbol for Fe1, Zn1, and Zn2 are represented by Schläfli symbols, $\{4^5.6^5\}$, $\{4^4.6^{10}.8\}$, and $\{4^3.6^3\}$. Further

dx.doi.org/10.1021/ic401657d | *Inorg. Chem.* 2013, 52, 11385−11397

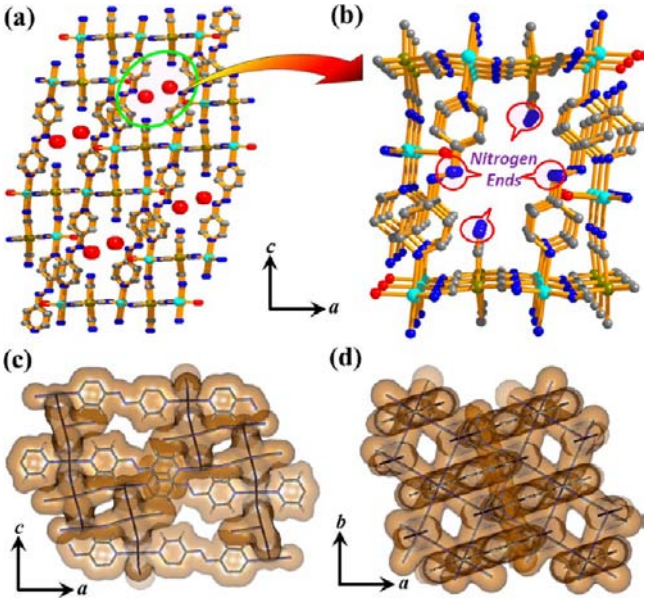

Figure 4. (a) The 2D sheets are linked by azpy linkers to generate a 3D framework of **3** showing the channels along the crystallographic *b* axis occupied by water molecules. (b) Zoomed view of the pore decorated with azo functional groups and free CN groups. Views of the pore in **3** after removing the guest water molecules: (c) along the *b* axis, and (d) along the *c* axis.

examination shows that **3** adopts an unprecedented network topology with the Schläfli symbol $\{4^3.6^3\}_2\{4^4.6^{10}.8\}\{4^5.6^5\}_2$. azpy molecules engage themselves in a weak $\pi\cdots\pi$ interaction (cg···cg distances are in the range of 4.124 Å) along the *b* direction, whereas the Fe1 and Zn2 centers are interacting with each other through O1−H···O2W and O2W−H···N4 H-bonding. The removal of guest water molecules results in small rectangular channels that account for 27% void volume in the framework (5.2 × 3.1 $Å^2$ and 3.9 × 3.9 $Å^2$) (Figure 4c,d) of compound **3**.

Framework Stability: Thermogravimetric (TG) and Powder X-ray Diffraction (PXRD) Analysis. Thermogravimetric analysis (TGA) and powder X-ray diffraction (PXRD) measurements at different temperatures were carried out to study the stability of the framework compounds. TGA of compounds **1**−**3** was performed in the temperature range of 30−650 °C under a nitrogen atmosphere. The TGA profile of compound **1** (Figure S5, Supporting Information) indicates a weight loss of 3.1% at 120 °C, which corroborates the removal of two guest water molecules (cal. 2.49%). The second step was observed at 210 °C with a weight loss of 24.8%, indicating the removal of all guest bipy and coordinated water molecules (cal. 25.3%). The desolvated framework is stable up to 245 °C. Compound **2** does not show any step in the TGA profile (Figure S6, Supporting Information) and gradually losses weight with increasing temperature. At ∼150 °C, it loses all guest water molecules (cal. 7.63%, obs. 7.30%) and finally transforms to an unidentified product. In the case of **3** (Figure S7, Supporting Information), a sharp decrease in weight was observed at 95 °C with a total loss of ∼10% (cal. 9.97%), suggesting the removal of all guest water molecules and that the dehydrated framework is stable up to 185 °C.

The PXRD patterns of compounds **1**−**3** are shown in Figure 5 and Figures S8 and S9 (Supporting Information), respectively. In all the compounds, good correspondence of

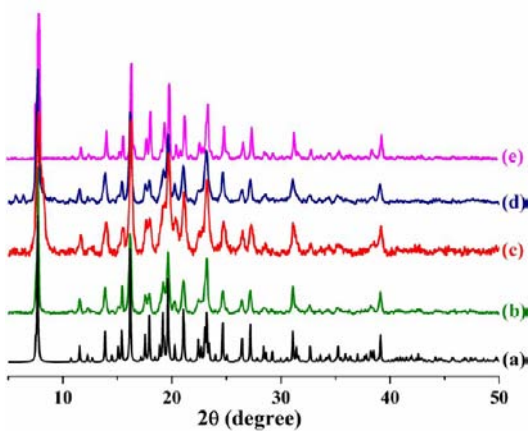

Figure 5. PXRD patterns of compound **1** in different states: (a) simulated, (b) as-synthesized, (c) heated at 175 °C and (d) rehydrated, and (e) compound **1** treated with the boiling water for 12 h.

the different peak positions in the simulated and as-synthesized patterns suggests the phase purity of the as-synthesized compounds. In the cases of **1′**−**3′**, the similarity of the PXRD patterns between as-synthesized and heated samples indicates that there is no significant structural change upon desolvation, though there is a trivial decrease in crystallinity that is reflected from the broadening of some peaks. The PXRD patterns of the rehydrated samples have not changed significantly even after exposing water vapor for 15 days, suggesting the framework stability in the presence of water vapor.

Permanent Porosity and Gas Storage Property. All the three compounds were subjected to N_2 adsorption at 77 K (Figure S10, Supporting Information). Compound **2** shows a typical type-II profile, obtained with the final uptake of 35 mL g^{-1}, suggesting only surface adsorption. However, in the cases of **1** and **3**, a combined isotherm of type I and type II was observed with a final uptake of 53 and 47 mL g^{-1}, respectively, suggesting the microporous nature of both the compounds. Hysteresis in the sorption profiles suggests the presence of a high diffusion barrier for N_2 in both the compounds. Interesting results were obtained in gas (CO_2, N_2, Ar, CH_4, and O_2) adsorption studies of the three compounds at 195 K, which suggests selective capture of CO_2 by all the three compounds (Figure 6). CO_2 adsorption isotherms of all compounds show a type-I profile with a significant amount of uptake at low-pressure regions. The steep uptake at the relatively low P/P_0 (∼0.04) region reveals a strong interaction of CO_2 with the pore surface. After $P/P_0 \approx 0.05$, the gradient of uptake profiles has been decreased and ended with a final volume uptake of 16.7 wt % (85 mL g^{-1}), 8.8 wt % (45 mL g^{-1}), and 16.8 wt % (88 mL g^{-1}) for **1′**, **2′**, and **3′**, respectively (Figure 6). Desorption curves of compounds **1′** and **3′** follow the adsorption one, whereas, for compound **2′**, the sorption profile shows a large hysteresis retaining 24 mL g^{-1} of CO_2 even at very low P/P_0 (0.001). This may be due to the strong interaction between the pendent pyridyl nitrogen atom and CO_2 molecules, which facilitate the kinetic trapping of gas molecules inside the pore of compound **2**, resulting in hysteresis and retaining of some CO_2 molecules (Figure S16, Supporting Information). The Langmuir surface area was calculated from CO_2 adsorption profiles that turned out to be 340, 160, and 273 m^2 g^{-1} for **1′**, **2′**, and **3′**, respectively. In the

dx.doi.org/10.1021/ic401657d | *Inorg. Chem.* 2013, 52, 11385−11397

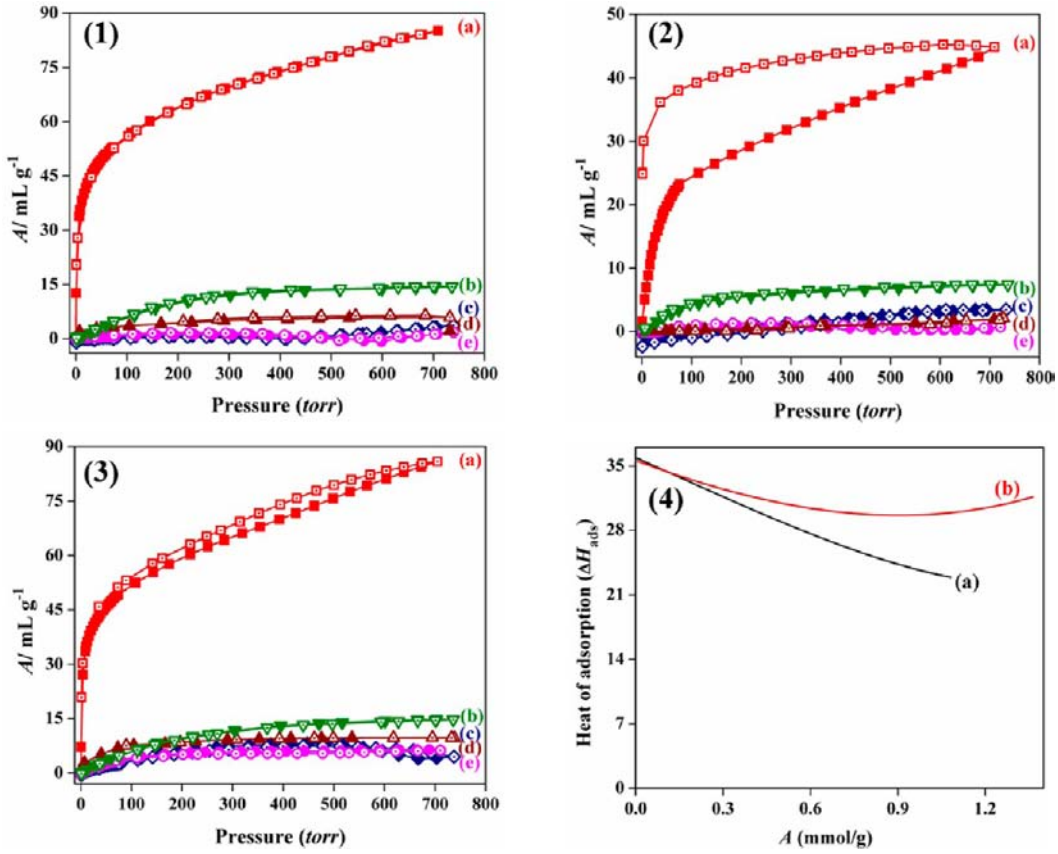

Figure 6. Gas adsorption isotherms of **1′**−**3′** at 195 K are shown in (1)−(3), respectively: (a) CO_2, (b) O_2, (c) CH_4, (d) Ar, and (e) N_2. Closed symbols and open symbols correspond to adsorption and desorption, respectively. (4) Change of enthalpy of adsorption for CO_2 with the increase of loading for **1′** (a) and **3′** (b) calculated based on adsorption at 273 and 293 K by using the virial equation (details of the calculation are given in the Supporting Information).

case of **2**, the smaller pore volume as well as the lesser void space as calculated from PLATON was also reflected in the lesser CO_2 uptake. Adsorption isotherms of other small molecules, such as Ar, O_2, CH_4, and N_2, were also measured at 195 K with **1′**−**3′**. They show a negligible amount of uptake compared to that for CO_2 (Figure 6), suggesting high selectivity in CO_2 uptake. In addition, we have also measured the CO_2 uptake capacity for **1′** and **3′** at temperatures of 273 and 293 K. The uptake amounts were found to be 30 and 24 mL g^{-1} for **1′**, whereas, for **3′**, it adsorbs 38 and 30 mL g^{-1} at the respective temperatures. To better understand the interactions between CO_2 and the dehydrated frameworks of **1** and **3** (i.e., **1′** and **3′**), we have calculated the zero coverage isosteric heat of adsorption (Q_{st}) using a virial equation (details are in the Supporting Information, Figures S11 and S12). As shown in Figure 6(4), the zero coverage isosteric heat of adsorptions were found to be 35.84 and 35.53 kJ mol^{-1} for **1′** and **3′**, respectively. The calculated Q_{st} values are comparable or even higher than some well-established CO_2-capturing MOFs,[34] entailing relatively stronger interactions between the CO_2 and the pore surface of **1′** and **3′**. The stronger interaction between CO_2 and the MOF surface is also reflected from the selectivity estimation of CO_2 over N_2 and CH_4 employing the IAST (Ideal Adsorbed Solution Theory) model[35] (Figure 7). At 273 K, for **1′** and **3′**, the predicted adsorption selectivities of CO_2 over N_2 for a bimolar (15:85) mixture of CO_2−N_2 are 16 and 62, respectively (Figure 7a,b). For an equimolar (50: 50) mixture of CO_2 and CH_4, the values turned out to be 18 and 13 at 273 K for **1′** and **3′**, respectively (Figure 7c,d). Compound **3′** exhibits better CO_2−N_2 selectivity compared to other reported MOFs,[34e,36] suggesting that it may have potential applications in the separation of CO_2 from a binary CO_2−N_2 mixture. It is very clear that all the factors, such as polar channels, high density of UMSs, and free nitrogen ends (from hanging cyanide ligands and pendent pyridyl nitrogen end), favor the inclusion of CO_2 molecules into the pores, whereas other small nonpolar molecules were completely excluded. This is also supported by the high values of enthalpy of CO_2 adsorption. This could also be correlated with the well-established fact that the electric field generated in the framework by UMSs and the aromatic π cloud interacts firmly with the quadrupole moment of CO_2 (-1.4×10^{-39} C m^2), causing a rapid uptake at low pressure.

A moderate surface area with a relatively polar pore surface based on unsaturated metal sites and free nitrogen ends further motivated us to examine their H_2-storage capacity at 77 K. Adsorption isotherms of **1′**−**3′** show typical type-I curves. Compounds **1′** and **3′** reveal a steep uptake at the low-pressure region with the final adsorption amount of 0.47 wt % (52.5 mL g^{-1}) and 0.7 wt % (78 mL g^{-1}), respectively (Figure 8(1), a−c). In the case of **2′**, the uptake amount gradually increases with increasing pressure and the desorption curve does not follow the adsorption one showing a small hysteresis. The final uptake value is about 24 mL g^{-1}, which corresponds to 0.22 wt % (Figure 8(1), b). We have also measured the zero coverage isosteric heats of hydrogen adsorption following the virial

dx.doi.org/10.1021/ic401657d | Inorg. Chem. 2013, 52, 11385−11397

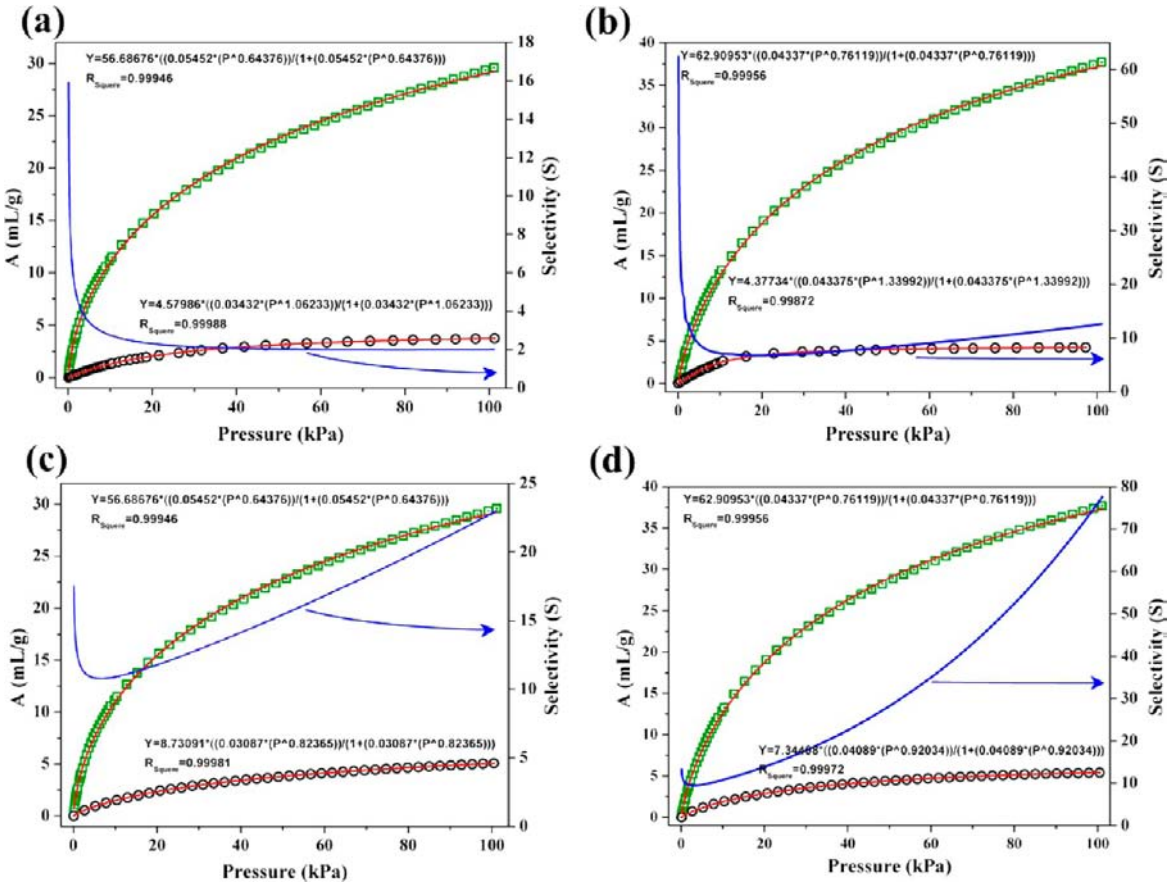

Figure 7. Langmuir–Freundlich fittings for (a, b) CO_2 (green square) and N_2 (black circle) isotherms measured at 273 K for compounds **1′** and **3′**, respectively. (c, d) CO_2 (green square) and CH_4 (black circle) isotherms measured at 273 K for compounds **1′** and **3′**, respectively. Blue curves correspond to the predicted adsorption selectivity for CO_2 over N_2 and CH_4, respectively, at the same temperature.

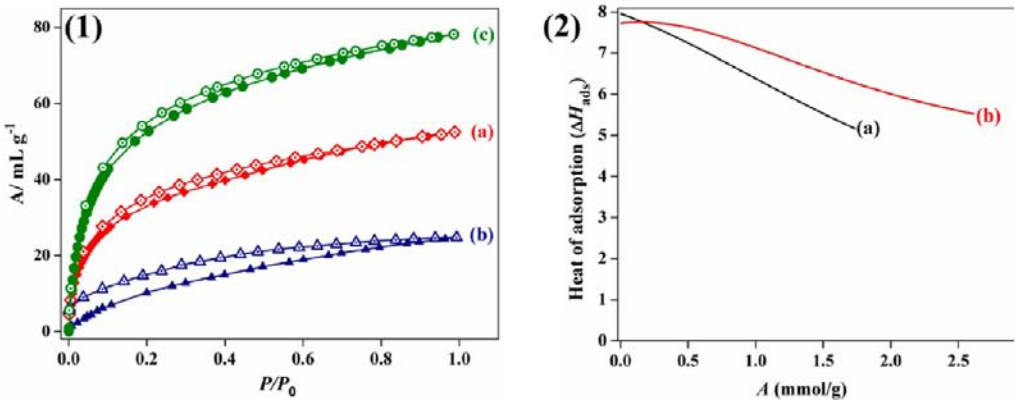

Figure 8. (1) H_2 adsorption isotherms of **1′** (a), **2′** (b), and **3′** (c) at 77 K. Closed symbols and open symbols correspond to adsorption and desorption, respectively. (2) Change of enthalpy of H_2 adsorption based on loading for **1′** (a) and **3′** (b) calculated using the 77 and 87 K data by using the virial equation (details of the calculation are given in the Supporting Information).

equation based on the adsorption profiles measured at 77 and 87 K. At the onset of adsorption, the enthalpies were calculated to be (details in the Supporting Information and Figures S13–S14) a value of 7.97 and 7.73 kJ mol^{-1} (Figure 8(2)) for **1′** and **3′**, respectively, which may be attributed to the interactions of H_2 molecules with open Zn sites, free cyanides, and the aromatic π cloud.

Furthermore, to check the stability of the dehydrated compounds (**1′**–**3′**) under humid conditions, we have measured the water adsorption isotherm at 298 K. All the compounds show a gradual uptake (Figures S17–S19, Supporting Information) of water with increasing pressure, and the corresponding final uptake values are 130, 59, and 103 mL g^{-1} (corresponding to 6, 2, and 5 molecules/formula unit), respectively, for **1′**–**3′**. Compounds **1′**–**3′** were also treated with boiling water for 12 h. The PXRD patterns (Figure 5e, Figures S8e and S9e, Supporting Information) of the resulting compounds do not show any significant change, which corresponds to the good stability of those materials under hydrothermal conditions.

dx.doi.org/10.1021/ic401657d | *Inorg. Chem.* 2013, 52, 11385–11397

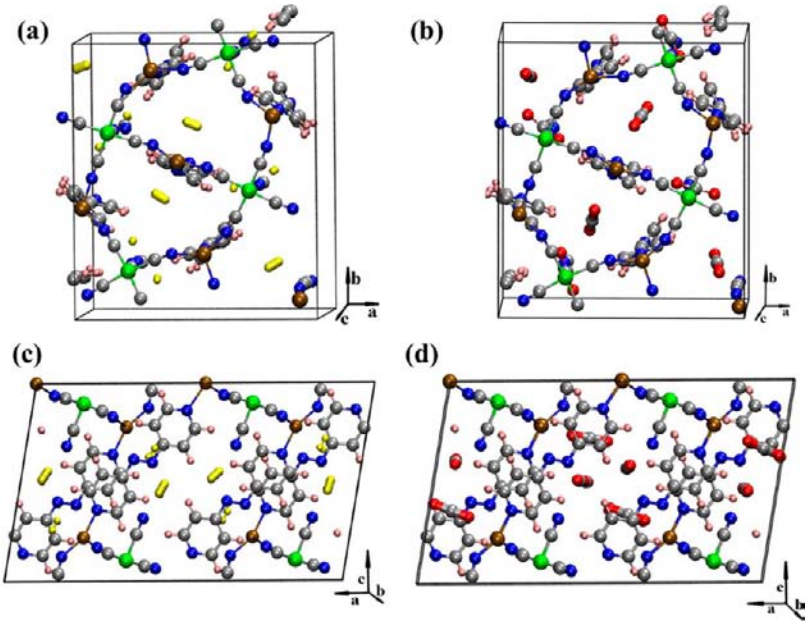

Figure 9. Locations of (a) H_2 and (b) CO_2 molecules in **1′** and of (c) H_2 and (d) CO_2 gas molecules in **3′**. Color codes for MOF atoms: silver - C, blue - N, pink - H, ochre - Zn, and green - Fe. H atoms in the H_2 molecule are yellow, while carbon and oxygen in CO_2 are in silver and red, respectively.

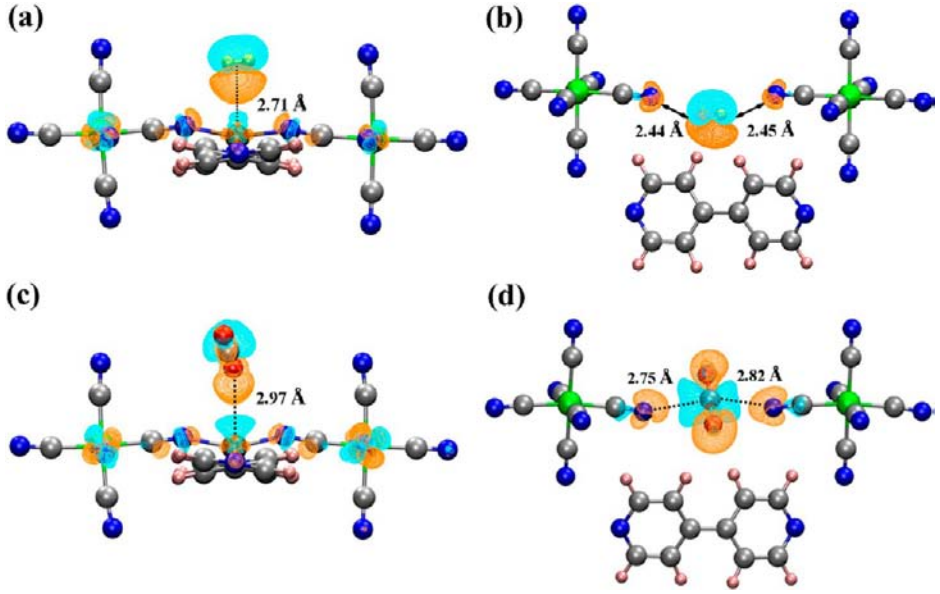

Figure 10. (a, b) H_2 interacting with the Zn and CN sites. (c, d) CO_2 interacting with Zn and CN sites in **1′**. Cyan and orange regions indicate decreased and increased electron densities, respectively, with respect to the isolated MOF and isolated gas molecule. Isosurface value is 4×10^{-4} a.u. Color codes for MOF atoms: silver - C, blue - N, pink - H, ochre - Zn, and green - Fe. H atoms in the H_2 molecule are yellow, while carbon and oxygen in CO_2 are in silver and red, respectively. The electron density differences were calculated for the entire MOF crystal, although only a part (fragment) of the MOF is shown for clarity.

To obtain an insight into the interaction between the gas molecule and dehydrated MOFs, we have performed calculations based on density functional theory. As discussed in the Experimental Section, adsorption sites for H_2 and CO_2 molecules were identified in **1′** and **3′** based on geometry optimization. Some of the H_2 positions in **1′** were identified based on the positions of solvent molecules in the as-synthesized MOF, and a few others were identified based on H_2 interactions with ligands, as reported in the literature.[5a] These locations in the simulation cell are displayed in Figure 9. The specific nature of interaction between the gas molecule and the framework can be understood through Figures 10 and 11, which exhibit the region of the MOF that is proximal to the gas molecule. For H_2 and CO_2 in **1′**, two distinct binding sites are possible: (i) the four-coordinated unsaturated Zn2 atom (with two ligand vacancies) and (ii) freely hanging CN groups. In fact, these are the sites at which the solvent water molecules are located in **1**. Thus, two H_2 molecules can ligate the Zn2 atom and two H_2 molecules could interact with a pair of free CN groups. However, in the latter, the site occupancy of one of the H_2 molecules can be expected to be 1/2, similar to that for the solvent present therein in the as-synthesized compound **1**.

dx.doi.org/10.1021/ic401657d | *Inorg. Chem.* 2013, 52, 11385−11397

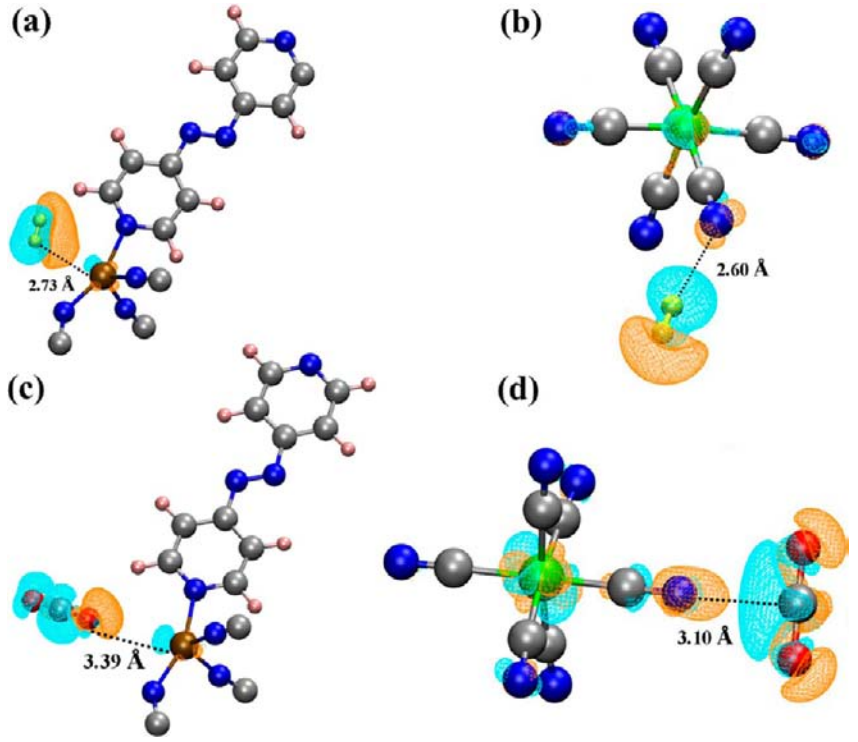

Figure 11. (a, b) H_2 interacting with the Zn and CN sites. (c, d) CO_2 interacting with Zn and CN sites in **3′**. Cyan and orange regions indicate decreased and increased electron densities, respectively, with respect to the isolated MOF and isolated gas molecule. Isosurface value is 4×10^{-4} a.u. Color codes for MOF atoms: silver - C, blue - N, pink - H, ochre - Zn, and green - Fe. H atoms in the H_2 molecule are yellow, while carbon and oxygen in CO_2 are in silver and red, respectively. The electron density differences were calculated for the entire MOF crystal, although only a part (fragment) of the MOF is shown for clarity.

Given that there are four CN groups in the formula unit, the maximum number of H_2 molecules that can be adsorbed in **1′** is five. High-pressure adsorption data for H_2 in **1′** saturates to an uptake value of 65 mL g^{-1}, which amounts to 3.2 H_2 molecules per formula unit (Figure S15, Supporting Information). The difference in the maximum uptake observed experimentally and that predicted from calculations could be due to possible distortion in the MOF structure upon desolvation, which has not been considered in theory. Another possibility could be inaccessible pores in experiment, which, too, could reduce the maximum gas uptake from the theoretical estimate. In the case of CO_2 in **1′**, two molecules are present coordinating the Zn atom, one molecule for a pair of CN groups, totaling to a maximum of four molecules of CO_2 per formula unit of **1′**.

For H_2 and CO_2 in **3′**, two distinct binding sites are possible: (i) the four-coordinated Zn2 atom (with one ligand vacancy) and (ii) freely hanging CN groups. A maximum of two molecules of H_2 can be present coordinating with two Zn metal atoms and two molecules can be present near the two CN groups, thus totaling to a maximum of four molecules of H_2 per formula unit of **3′**. A similar maximum number is obtained for CO_2 in **3′** as well. The H_2 molecule interacts with the CN group, with the latter donating a partial electronic charge to the σ1s MO of H_2. The same is also seen clearly in the case of the Zn−H_2 interaction where the long axis of the H_2 molecule is positioned laterally to the Zn atom. These are illustrated in Figures 10a and 11a for the two MOF compounds. CO_2 interacts simultaneously with the CN group as well as weakly with the C−H group of bipy. A Lewis acid−base interaction with CN is observed, with the carbon atom of CO_2 losing electronic charge partially to the nitrogen of CN. The interaction with the under-coordinated Zn site is through the oxygen atom of CO_2. Similar to the case of H_2, the Zn atom loses partial electronic charge to CO_2, as seen from Figures 10 and 11 for the two MOF compounds.

The binding energies calculated from the PBE-D3 approach compare very well against the experimentally obtained low coverage isosteric heat of adsorption. The results are displayed in Table 2. The calculated binding energies for H_2 and CO_2 in **1′** and for CO_2 in **3′** are within 5% of the experimental values. However, for H_2 adsorption in **3′**, a value of 14.7 kJ mol^{-1} is obtained compared to the experimental value of 7.73 kJ/mol. The calculated energy improved to 9.9 kJ/mol upon inclusion of the C9 term[24] (3-body term) within the D3 vdW description. Also pertinent to note are the positive binding

Table 2. Calculated Binding Energies of H_2 and CO_2 with the Frameworks[a]

MOF	method	gas	binding energy (kJ/mol)	
			at Zn site	at CN site
1′	PBE-D3	H_2 (PBE only)	−6.25	−4.00
		H_2	−7.16	−8.50
		CO_2	−34.64	−34.51
3′	PBE-D3	H_2 (PBE only)	−2.80	−3.90
		H_2	−14.78	−14.98
		H_2 (including 3-body vdW term)	−9.96	−11.10
		CO_2	−35.26	−35.60

[a]The binding energies for N_2 and CH_4 at the Zn site of **1′** calculated using the PBE functional were +1.8 and +0.7 kJ/mol, respectively.

dx.doi.org/10.1021/ic401657d | *Inorg. Chem.* 2013, 52, 11385−11397

energy values for N_2 and CH_4 in **1′** using the PBE functional. These correlate well with the much reduced uptake of these gases, as seen in Figure 6.

CONCLUSIONS

We have successfully synthesized three metal−organic frameworks with the self-assembly of Zn(II), $[Fe(CN)_6]^{3-}$, and organic linkers (bipy, azpy). A systematic study of structural variation was performed by changing the organic linker as well as their concentrations. Compounds **1** and **3** are fascinating from the structural point of view as they act as a biporous host. At 195 K, all the compounds selectively adsorb CO_2 while they completely exclude other small molecules, such as N_2, Ar, O_2, and CH_4. Moreover, the desolvated framework of **1** and **3** shows selectivity of CO_2 over N_2, indicating that they may serve as prototypes for future materials designed for CO_2 capture processes. The heat of hydrogen adsorption at cryogenic temperature reveals moderate interaction of H_2 molecules with the unsaturated Zn(II) site as well as with the pore surface. The observations have been confirmed through density functional theory calculations that included empirical van der Waals corrections. We have successfully varied the structure and their properties with the change of organic linkers and linker concentration. It is noteworthy that the polar pore surface based on a high density of UMSs and polar binding functional groups in these frameworks provides an excellent platform to study H_2 and CO_2 storage properties, which will essentially pave the way for the synthesis of future novel high-performance adsorbent materials.

ASSOCIATED CONTENT

Supporting Information

IR spectra of compounds **1**−**3** at different states, powder X-ray diffraction (PXRD) analyses (**2**−**3**), thermogravimetric analysis (TGA) (**1**−**3**), details of adsorption analysis and plots, computational details, selected bond lengths and angles of compounds **1**−**3**, and extensive figures of compounds **1** and **2**. This material is available free of charge via the Internet at http://pubs.acs.org.

AUTHOR INFORMATION

Corresponding Authors

*E-mail: bala@jncasr.ac.in (S.B.).

*E-mail: tmaji@jncasr.ac.in (T.K.M.). Tel: (+91)-80-2208-2826. Fax: (+91)-80-2208-2766.

Notes

The authors declare no competing financial interest.

ACKNOWLEDGMENTS

T.K.M. gratefully acknowledges a Sheikh Saqr fellowship. A.H. acknowledges JNCASR and DST for a scholarship. We would like to thank the Centre for Development of Advanced Computing (C-DAC) - Bangalore, and the CSIR Fourth Paradigm Institute (CSIR-4PI) - Bangalore for providing computational resources.

REFERENCES

(1) (a) Chen, B. L.; Xiang, S. C.; Qian, G. D. *Acc. Chem. Res.* **2010**, *43*, 1115−1124. (b) Janiak, C.; Vieth, J. K. *New J. Chem.* **2010**, *34*, 2366−2388. (c) Horike, S.; Shimomura, S.; Kitagawa, S. *Nat. Chem.* **2009**, *1*, 695−704. (d) Kitagawa, S.; Kitaura, R.; Noro, S. *Angew. Chem., Int. Ed.* **2004**, *43*, 2334−2375. (e) Kuppler, R. J.; Timmons, D. J.; Fang, Q. R.; Li, J. R.; Makal, T. A.; Young, M. D.; Yuan, D. Q.; Zhao, D.; Zhuang, W. J.; Zhou, H. C. *Coord. Chem. Rev.* **2009**, *253*, 3042−3066. (f) Meek, S. T.; Greathouse, J. A.; Allendorf, M. D. *Adv. Mater.* **2011**, *23*, 249−267. (g) Ma, L. Q.; Lin, W. B. Designing Metal-Organic Frameworks for Catalytic Applications. In *Functional Metal-Organic Frameworks: Gas Storage, Separation and Catalysis*; Schröder, M., Ed.; Topics in Current Chemistry; Springer-Verlag: Berlin, Germany, **2010**; Vol. *293*, pp 175−205. (h) Paz, F. A. A.; Klinowski, J.; Vilela, S. M. F.; Tome, J. P. C.; Cavaleiro, J. A. S.; Rocha, J. *Chem. Soc. Rev.* **2012**, *41*, 1088−1110. (i) Seo, J.; Sakamoto, H.; Matsuda, R.; Kitagawa, S. *J. Nanosci. Nanotechnol.* **2010**, *10*, 3−20. (j) Yang, R.; Li, L.; Xiong, Y.; Li, J.-R.; Zhou, H.-C.; Su, C.-Y. *Chem.—Asian J.* **2010**, *5*, 2358−2368. (k) Hayashi, H.; Cote, A. P.; Furukawa, H.; O'Keeffe, M.; Yaghi, O. M. *Nat. Mater.* **2007**, *6*, 501−506. (l) Doonan, C. J.; Morris, W.; Furukawa, H.; Yaghi, O. M. *J. Am. Chem. Soc.* **2009**, *131*, 9492−9493.

(2) (a) Uemura, K.; Kitagawa, S.; Fukui, K.; Saito, K. *J. Am. Chem. Soc.* **2004**, *126*, 3817−3828. (b) Choi, E.-Y.; Park, K.; Yang, C.-M.; Kim, H.; Son, J.-H.; Lee, S. W.; Lee, Y. H.; Min, D.; Kwon, Y.-U. *Chem.—Eur. J.* **2004**, *10*, 5535−5540. (c) Matsuda, R.; Kitaura, R.; Kitagawa, S.; Kubota, Y.; Belosludov, R. V.; Kobayashi, T. C.; Sakamoto, H.; Chiba, T.; Takata, M.; Kawazoe, Y.; Mita, Y. *Nature* **2005**, *436*, 238−241. (d) Kepert, C. J. *Chem. Commun.* **2006**, 695−700. (e) Ma, S.; Zhou, H.-C. *J. Am. Chem. Soc.* **2006**, *128*, 11734−11735. (f) Sudik, A. C.; Cote, A. P.; Wong-Foy, A. G.; O'Keeffe, M.; Yaghi, O. M. *Angew. Chem., Int. Ed.* **2006**, *45*, 2528−2533. (g) Mulfort, K. L.; Hupp, J. T. *J. Am. Chem. Soc.* **2007**, *129*, 9604−9605. (h) Shimomura, S.; Horike, S.; Matsuda, R.; Kitagawa, S. *J. Am. Chem. Soc.* **2007**, *129*, 10990−10991. (i) Wang, Z.; Cohen, S. M. *J. Am. Chem. Soc.* **2007**, *129*, 12368−12369.

(3) (a) Chen, B. L.; Ockwig, N. W.; Millward, A. R.; Contreras, D. S.; Yaghi, O. M. *Angew. Chem., Int. Ed.* **2005**, *44*, 4745−4749. (b) Dinca, M.; Long, J. R. *J. Am. Chem. Soc.* **2005**, *127*, 9376−9377. (c) Gedrich, K.; Senkovska, I.; Klein, N.; Stoeck, U.; Henschel, A.; Lohe, M. R.; Baburin, I. A.; Mueller, U.; Kaskel, S. *Angew. Chem., Int. Ed.* **2010**, *49*, 8489−8492. (d) Li, Y.; Yang, R. T. *J. Am. Chem. Soc.* **2005**, *128*, 726−727. (e) Li, Y.-S.; Liang, F.-Y.; Bux, H.; Feldhoff, A.; Yang, W.-S.; Caro, J. *Angew. Chem., Int. Ed.* **2010**, *49*, 548−551. (f) Lin, X.; Jia, J.; Zhao, X.; Thomas, K. M.; Blake, A. J.; Walker, G. S.; Champness, N. R.; Hubberstey, P.; Schröder, M. *Angew. Chem., Int. Ed.* **2006**, *45*, 7358−7364. (g) Panella, B.; Hirscher, M.; Pütter, H.; Müller, U. *Adv. Funct. Mater.* **2006**, *16*, 520−524. (h) Sumida, K.; Brown, C. M.; Herm, Z. R.; Chavan, S.; Bordiga, S.; Long, J. R. *Chem. Commun.* **2011**, *47*, 1157−1159. (i) Sumida, K.; Hill, M. R.; Horike, S.; Dailly, A.; Long, J. R. *J. Am. Chem. Soc.* **2009**, *131*, 15120−15121.

(4) (a) Ferey, G.; Mellot-Draznieks, C.; Serre, C.; Millange, F.; Dutour, J.; Surble, S.; Margiolaki, I. *Science* **2005**, *309*, 2040−2042. (b) Huang, X.-C.; Lin, Y.-Y.; Zhang, J.-P.; Chen, X.-M. *Angew. Chem., Int. Ed.* **2006**, *45*, 1557−1559. (c) Park, K. S.; Ni, Z.; Cote, A. P.; Choi, J. Y.; Huang, R. D.; Uribe-Romo, F. J.; Chae, H. K.; O'Keeffe, M.; Yaghi, O. M. *Proc. Natl. Acad. Sci. U.S.A.* **2006**, *103*, 10186−10191. (d) Tian, Y.-Q.; Zhao, Y.-M.; Chen, Z.-X.; Zhang, G.-N.; Weng, L.-H.; Zhao, D.-Y. *Chem.—Eur. J.* **2007**, *13*, 4146−4154. (e) Agarwal, R. A.; Aijaz, A.; Sañudo, C.; Xu, Q.; Bharadwaj, P. K. *Cryst. Growth Des.* **2013**, *13*, 1238−1245. (f) Agarwal, R. A.; Aijaz, A.; Ahmad, M.; Sañudo, E. C.; Xu, Q.; Bharadwaj, P. K. *Cryst. Growth Des.* **2012**, *12*, 2999−3005.

(5) (a) Murray, L. J.; Dinca, M.; Long, J. R. *Chem. Soc. Rev.* **2009**, *38*, 1294−1314. (b) Achmann, S.; Hagen, G.; Kita, J.; Malkowsky, I.; Kiener, C.; Moos, R. *Sensors* **2009**, *9*, 1574−1589. (c) Horcajada, P.; Serre, C.; Maurin, G.; Ramsahye, N. A.; Balas, F.; Vallet-Regí, M.; Sebban, M.; Taulelle, F.; Férey, G. *J. Am. Chem. Soc.* **2008**, *130*, 6774−6780. (d) Lee, J.; Farha, O. K.; Roberts, J.; Scheidt, K. A.; Nguyen, S. T.; Hupp, J. T. *Chem. Soc. Rev.* **2009**, *38*, 1450−1459. (e) Li, J.-R.; Kuppler, R. J.; Zhou, H.-C. *Chem. Soc. Rev.* **2009**, *38*, 1477−1504. (f) Maspoch, D.; Ruiz-Molina, D.; Veciana, J. *Chem. Soc. Rev.* **2007**, *36*, 770−818. (g) Thallapally, P. K.; Fernandez, C. A.; Motkuri, R. K.; Nune, S. K.; Liu, J.; Peden, C. H. F. *Dalton Trans.* **2010**, *39*, 1692−1694. (h) Thallapally, P. K.; Motkuri, R. K.; Fernandez, C. A.; McGrail, B. P.; Behrooz, G. S. *Inorg. Chem.* **2010**, *49*, 4909−4915.

(6) van den Berg, A. W. C.; Arean, C. O. *Chem. Commun.* **2008**, 668−681.
(7) Eberle, U.; Felderhoff, M.; Schüth, F. *Angew. Chem., Int. Ed.* **2009**, *48*, 6608−6630.
(8) Rowsell, J. L. C.; Yaghi, O. M. *Angew. Chem., Int. Ed.* **2005**, *44*, 4670−4679.
(9) (a) Mulfort, K. L.; Hupp, J. T. *Inorg. Chem.* **2008**, *47*, 7936−7938. (b) Mohapatra, S.; Hembram, K. P. S. S.; Waghmare, U.; Maji, T. K. *Chem. Mater.* **2009**, *21*, 5406−5412. (c) Mulfort, K. L.; Farha, O. K.; Stern, C. L.; Sarjeant, A. A.; Hupp, J. T. *J. Am. Chem. Soc.* **2009**, *131*, 3866−3868.
(10) (a) Cheon, Y. E.; Suh, M. P. *Chem. Commun.* **2009**, 2296−2298. (b) Dincă, M.; Long, J. R. *Angew. Chem., Int. Ed.* **2008**, *47*, 6766−6779. (c) Kong, X.; Scott, E.; Ding, W.; Mason, J. A.; Long, J. R.; Reimer, J. A. *J. Am. Chem. Soc.* **2012**, *134*, 14341−14344. (d) Lin, L.-C.; Kim, J.; Kong, X.; Scott, E.; McDonald, T. M.; Long, J. R.; Reimer, J. A.; Smit, B. *Angew. Chem., Int. Ed.* **2013**, *52*, 4410−4413. (e) Nijem, N.; Kong, L.; Zhao, Y.; Wu, H.; Li, J.; Langreth, D. C.; Chabal, Y. J. *J. Am. Chem. Soc.* **2011**, *133*, 4782−4784. (f) Sumida, K.; Her, J.-H.; Dincă, M.; Murray, L. J.; Schloss, J. M.; Pierce, C. J.; Thompson, B. A.; FitzGerald, S. A.; Brown, C. M.; Long, J. R. *J. Phys. Chem. C* **2011**, *115*, 8414−8421.
(11) Kanoo, P.; Reddy, S. K.; Kumari, G.; Haldar, R.; Narayana, C.; Balasubramanian, S.; Maji, T. K. *Chem. Commun.* **2012**, *48*, 8487−8489.
(12) (a) Suri, M.; Dornfeld, M.; Ganz, E. *J. Chem. Phys.* **2009**, *131*, 174703. (b) Nijem, N.; Veyan, J.-F.; Kong, L.; Wu, H.; Zhao, Y.; Li, J.; Langreth, D. C.; Chabal, Y. J. *J. Am. Chem. Soc.* **2010**, *132*, 14834−14848. (c) Jayaramulu, K.; Reddy, S. K.; Hazra, A.; Balasubramanian, S.; Maji, T. K. *Inorg. Chem.* **2012**, *51*, 7103−7111. (d) Klontzas, E.; Tylianakis, E.; Froudakis, G. E. *J. Phys. Chem. Lett.* **2011**, *2*, 1824−1830.
(13) (a) Arenillas, A.; Smith, K. M.; Drage, T. C.; Snape, C. E. *Fuel* **2005**, *84*, 2204−2210. (b) Holloway, S. *Energy* **2005**, *30*, 2318−2333. (c) White, C. M.; Smith, D. H.; Jones, K. L.; Goodman, A. L.; Jikich, S. A.; LaCount, R. B.; DuBose, S. B.; Ozdemir, E.; Morsi, B. I.; Schroeder, K. T. *Energy Fuels* **2005**, *19*, 659−724.
(14) (a) Noro, S.-i.; Tanaka, D.; Sakamoto, H.; Shimomura, S.; Kitagawa, S.; Takeda, S.; Uemura, K.; Kita, H.; Akutagawa, T.; Nakamura, T. *Chem. Mater.* **2009**, *211*, 3346−3355. (b) Noro, S.-i.; Hijikata, Y.; Inukai, M.; Fukushima, T.; Horike, S.; Higuchi, M.; Kitagawa, S.; Akutagawa, T.; Nakamura, T. *Inorg. Chem.* **2012**, *52*, 280−285. (c) Motkuri, R. K.; Thallapally, P. K.; Nune, S. K.; Fernandez, C. A.; McGrail, B. P.; Atwood, J. L. *Chem. Commun.* **2011**, *47*, 7077−7079.
(15) (a) Kanoo, P.; Ghosh, A. C.; Cyriac, S. T.; Maji, T. K. *Chem.—Eur. J.* **2012**, *18*, 237−244. (b) Kanoo, P.; Matsuda, R.; Kitaura, R.; Kitagawa, S.; Maji, T. K. *Inorg. Chem.* **2012**, *51*, 9141−9143. (c) Haldar, R.; Maji, T. K. *CrystEngComm* **2012**, *14*, 684−690. (d) Haldar, R.; Narayan, R. P.; Maji, T. K. *Indian J. Chem., Sect. A: Inorg., Bio-inorg., Phys., Theor. Anal. Chem.* **2012**, *51A*, 1231−1237. (e) Kumar, R.; Jayaramulu, K.; Maji, T. K.; Rao, C. N. R. *Chem. Commun.* **2013**, *49*, 4947−4949. (f) Mohapatra, S.; Rajeswaran, B.; Chakraborty, A.; Sundaresan, A.; Maji, T. K. *Chem. Mater.* **2013**, *25*, 1673−1679. (g) Jayaramulu, K.; Kanoo, P.; George, S. J.; Maji, T. K. *Chem. Commun.* **2010**, *46*, 7906−7908. (h) Hazra, A.; Kanoo, P.; Maji, T. K. *Chem. Commun.* **2011**, *47*, 538−540. (i) Maji, T. K.; Pal, S.; Gurunatha, K. L.; Govindaraj, A.; Rao, C. N. R. *Dalton Trans.* **2009**, 4426−4428.
(16) Brown, E. V.; Granneman, G. R. *J. Am. Chem. Soc.* **1975**, *97*, 621−627.
(17) *SMART (V 5.628) SAINT (V 6.45a), XPREP, SHELXTL*; Bruker AXS Inc.: Madison, WI, 2004.
(18) Sheldrick, G. M. *SADABS: Empirical Absorption Correction Program*; University of Göttingen: Göttingen, Germany, 1997.
(19) Altomare, A.; Cascarano, G.; Giacovazzo, C.; Guagliardi, A. *J. Appl. Crystallogr.* **1993**, *26*, 343−350.
(20) Sheldrick, G. M. *SHELXL 97: Program for the Solution of Crystal Structure*; University of Göttingen: Göttingen, Germany, 1997.
(21) Spek, A. *J. Appl. Crystallogr.* **2003**, *36*, 7−13.
(22) Farrugia, L. *J. Appl. Crystallogr.* **1999**, *32*, 837−838.
(23) (a) VandeVondele, J.; Krack, M.; Mohamed, F.; Parrinello, M.; Chassaing, T.; Hutter, J. *Comput. Phys. Commun.* **2005**, *167*, 103−128. (b) Hutter, J.; Iannuzzi, M.; Schiffmann, F.; VandeVondele, J. *Wiley Interdiscip. Rev.: Comput. Mol. Sci.* **2013**, DOI: 10.1002/wcms.1159.
(24) Elstner, M.; Porezag, D.; Jungnickel, G.; Elsner, J.; Haugk, M.; Frauenheim, T.; Suhai, S.; Seifert, G. *Phys. Rev. B* **1998**, *58*, 7260−7268.
(25) Perdew, J. P.; Burke, K.; Ernzerhof, M. *Phys. Rev. Lett.* **1996**, *77*, 3865−3868.
(26) Grimme, S. *J. Comput. Chem.* **2006**, *27*, 1787−1799.
(27) Grimme, S.; Antony, J.; Ehrlich, S.; Krieg, H. *J. Chem. Phys.* **2010**, *132*, 154104.
(28) (a) VandeVondele, J.; Hutter, J. *J. Chem. Phys.* **2007**, *127*, 114105. (b) Lee, C.; Yang, W.; Parr, R. G. *Phys. Rev. B* **1988**, *37*, 785−789. (c) Becke, A. D. *Phys. Rev. A* **1988**, *38*, 3098−3100.
(29) Zhou, W.; Wu, H.; Yildirim, T. *J. Am. Chem. Soc.* **2008**, *130*, 15268−15269.
(30) Humphrey, W.; Dalke, A.; Schulten, K. *J. Mol. Graphics* **1996**, *14*, 33−38.
(31) (a) Macrae, C. F.; Edgington, P. R.; McCabe, P.; Pidcock, E.; Shields, G. P.; Taylor, R.; Towler, M.; van de Streek, J. *J. Appl. Crystallogr.* **2006**, *39*, 453−457. (b) http://www.ccdc.cam.ac.uk/Solutions/CSDSystem/Pages/Mercury.aspx.
(32) Dennington, R.; Keith, T.; Millam, J. *GaussView*, Version 5; Semichem Inc.: Shawnee Mission, KS, 2009.
(33) (a) Blatov, V. A.; Carlucci, L.; Ciani, G.; Proserpio, D. M. *CrystEngComm* **2004**, *6*, 377−395. (b) Blatov, V. A.; Shevchenko, A. P.; Serezhkin, V. N. *J. Appl. Crystallogr.* **2000**, *33*, 1193.
(34) (a) Bourrelly, S.; Llewellyn, P. L.; Serre, C.; Millange, F.; Loiseau, T.; Férey, G. *J. Am. Chem. Soc.* **2005**, *127*, 13519−13521. (b) Hou, L.; Shi, W.-J.; Wang, Y.-Y.; Guo, Y.; Jin, C.; Shi, Q.-Z. *Chem. Commun.* **2011**, *47*, 5464−5466. (c) Wu, H.; Reali, R. S.; Smith, D. A.; Trachtenberg, M. C.; Li, J. *Chem.—Eur. J.* **2010**, *16*, 13951−13954. (d) Kim, T. K.; Suh, M. P. *Chem. Commun.* **2011**, *47*, 4258−4260. (e) Park, H. J.; Suh, M. P. *Chem. Sci.* **2013**, *4*, 685−690. (f) Yuan, D.; Zhao, D.; Sun, D.; Zhou, H.-C. *Angew. Chem., Int. Ed.* **2010**, *49*, 5357−5361. (g) Huang, Y.-L.; Gong, Y.-N.; Jiang, L.; Lu, T.-B. *Chem. Commun.* **2013**, *49*, 1753−1755.
(35) (a) Myers, A. L.; Prausnitz, J. M. *AlChE J.* **1965**, *11*, 121−127. (b) Peng, J.; Ban, H.; Zhang, X.; Song, L.; Sun, Z. *Chem. Phys. Lett.* **2005**, *401*, 94−98. (c) Bae, Y.-S.; Mulfort, K. L.; Frost, H.; Ryan, P.; Punnathanam, S.; Broadbelt, L. J.; Hupp, J. T.; Snurr, R. Q. *Langmuir* **2008**, *24*, 8592−8598.
(36) Zheng, B.; Bai, J.; Duan, J.; Wojtas, L.; Zaworotko, M. J. *J. Am. Chem. Soc.* **2010**, *133*, 748−751.